Topology-Optimized Multilayered Metaoptics

Zin Lin,[1,*] Benedikt Groever,[1] Federico Capasso,[1] Alejandro W. Rodriguez,[2] and Marko Lončar[1]
[1]*John A. Paulson School of Engineering and Applied Sciences, Harvard University, Cambridge, Massachusetts 02138, USA*
[2]*Department of Electrical Engineering, Princeton University, Princeton, New Jersey 08544, USA*

(Received 17 June 2017; revised manuscript received 23 February 2018; published 20 April 2018)

We propose a general topology-optimization framework for metasurface inverse design that can automatically discover highly complex multilayered metastructures with increased functionalities. In particular, we present topology-optimized multilayered geometries exhibiting angular phase control, including a single-piece nanophotonic metalens with angular aberration correction, as well as an angle-convergent metalens that focuses light onto the same focal spot regardless of the angle of incidence.

DOI: 10.1103/PhysRevApplied.9.044030

I. INTRODUCTION

Phase-gradient metasurfaces [1] have recently received widespread attention due to their successful applications in important technologies such as beam steering, imaging, and holography [2–4]. Although they offer many advantages in terms of size and scaling over traditional refractive bulk optics, their capabilities are limited with respect to spectral and angular control [5,6]. Theoretical analysis of ultrathin metasurfaces suggests that, to circumvent such limitations, it might be necessary to employ exotic elements such as active permittivities (e.g., optical gain), bianisotropy, magnetic materials, or even nonlocal response [5]. Although materials with such properties might be found in the rf regime, they are not readily available at optical frequencies. Alternatively, device functionalities may be enhanced by increasingly complex geometric design. For instance, multifunctional devices have been demonstrated by cascading a few layers of metasurfaces, each of which comprises typical dielectric materials [7,8]. So far, most of these multilayered metastructures (MMSs) fall into a category of structures where the layers are sufficiently far apart from each other and can be considered independently.

In this article, we introduce a different class of MMSs involving several tightly spaced layers which allow richer physical interactions within and between layers and thereby offer increased functionality. The key property of these MMSs is that the layers cannot be treated independently of each other but must be considered integrally in the design process. Such a consideration often leads to a greatly extended design space that cannot be handled by traditional design methods, which rely on precompiled libraries of intuitive geometrical elements. Below, we propose a general topology-optimization (TO) framework that can automatically discover highly complex MMSs with broad functionalities. As a proof of concept, we present two TO multilayered geometries exhibiting angular phase control: a single-piece nanophotonic metalens with angular aberration correction [Fig. 1(a)] and an angle-convergent metalens that focuses light onto the same focal spot regardless of incident angle [Fig. 1(b)].

II. INVERSE-DESIGN FORMULATION

TO is an efficient computational technique that can handle an extensive design space, considering the dielectric permittivity at every spatial point as a degree of freedom (DOF) [9,10]. A typical TO electromagnetic problem can be written as

$$\max_{\{\bar{\epsilon}\}} \mathcal{F}(\mathbf{E};\bar{\epsilon}), \tag{1}$$

$$\mathcal{G}(\mathbf{E};\bar{\epsilon}) \le 0, \tag{2}$$

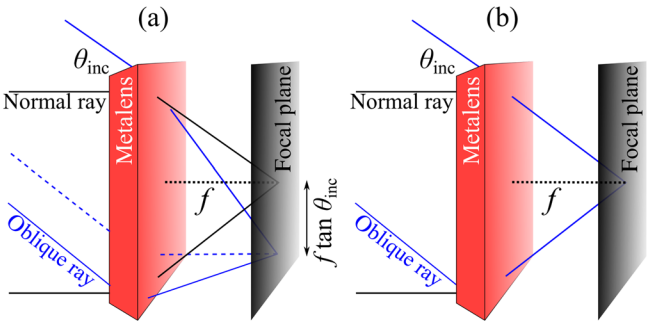

FIG. 1. Schematics (not to scale) of (a) a single-piece nanophotonic aberration-corrected metalens and (b) an angle-convergent metalens. The metalens ensures diffraction-limited focusing under general oblique incidence θ_{inc} either (a) onto a laterally shifted focal spot or (b) onto the same on-axis focal spot.

*zinlin@g.harvard.edu

$$0 \le \bar{\epsilon} \le 1. \tag{3}$$

Here, the DOFs $\{\bar{\epsilon}\}$ are related to the position-dependent dielectric profile via $\epsilon(\mathbf{r}) = (\epsilon_{\mathrm{st}} - \epsilon_{\mathrm{bg}})\bar{\epsilon}(\mathbf{r}) + \epsilon_{\mathrm{bg}}$, where $\epsilon_{\mathrm{st\,(bg)}}$ denotes the relative permittivity of the structural (background) dielectric material. While $\bar{\epsilon}$ may take intermediate values between 0 and 1, one can ensure a binary (digital) structure via penalization and filter projection methods [10]. The objective $\mathcal{F}$ and constraint $\mathcal{G}$ are often functions of the electric field $\mathbf{E}$, a solution of Maxwell's equation,

$$\nabla \times \frac{1}{\mu}\nabla \times \mathbf{E} - \epsilon(\mathbf{r})\frac{\omega^2}{c^2}\mathbf{E} = i\omega\mathbf{J}, \tag{4}$$

which yields the steady-state $\mathbf{E}(\mathbf{r};\omega)$ in response to incident currents $\mathbf{J}(\mathbf{r},\omega)$ at a given frequency ω. While the solution of Eq. (4) is straightforward and commonplace, the key to making optimization problems tractable is to obtain a fast-converging and computationally efficient adjoint formulation of the problem together with powerful mathematical programming routines such as the method of moving asymptotes [11,12]. Within the scope of TO, the key to formulating a tractable optimization problem involves efficient calculations of the derivatives $\{(\partial\mathcal{F})/[\partial\bar{\epsilon}(\mathbf{r})]\}, \{(\partial\mathcal{G})/[\partial\bar{\epsilon}(\mathbf{r})]\}$ at every spatial point $\mathbf{r}$, performed by exploiting the adjoint-variable method [10].

Recently, inverse-design techniques based on TO have been successfully applied to a variety of photonic systems including on-chip mode splitters, nonlinear frequency converters, and Dirac-cone photonic crystals [10,13–20]. However, to the best of our knowledge, there is an apparent lack of large-scale computational techniques specifically tailored for metasurface design, with the possible exception of Ref. [21], which is limited to grating deflectors. Here, we introduce a general optimization framework for designing a generic meta-optics device, single or multilayered, with an arbitrary phase response. The key to our formulation is the familiar superposition principle: given a desired phase profile $\phi(\mathbf{r})$, the ideal wave front $e^{i\phi(\mathbf{r})}$ and the complex electric field $E(\mathbf{r})$ will constructively interfere if and only if their phase difference vanishes. Defining $E(\mathbf{r}) = \mathbf{E}(\mathbf{r}) \cdot \hat{\mathbf{e}}$ for a given polarization $\hat{\mathbf{e}}$, we define the following optimization function:

$$\mathcal{F}(\bar{\epsilon}) = \frac{1}{V}\int \frac{|E(\mathbf{r}) + e^{i\phi(\mathbf{r})}|^2 - |E(\mathbf{r})|^2 - 1}{2|E(\mathbf{r})|}\,d\mathbf{r}, \tag{5}$$

where $V = \int d\mathbf{r}$ and the spatial integration is performed over a reference plane (typically one or two wavelengths away from the metadevice) where $\phi(\mathbf{r})$ is defined. Note that $\mathcal{F}$ is none other than a spatially averaged cosine of the phase difference between $e^{i\phi(\mathbf{r})}$ and $E(\mathbf{r})$,

$$\mathcal{F}(\bar{\epsilon}) = \frac{1}{V}\int \cos\left[\arg E(\mathbf{r}) - \phi(\mathbf{r})\right]d\mathbf{r},$$

with the property $\mathcal{F} \le 1$. Therefore, $\mathcal{F}$ can be used to gauge and characterize the performance of the device under construction, with $\mathcal{F} \approx 1$ indicating that the algorithm has converged to an optimal solution. In practice, the optimization algorithms discover devices with $\mathcal{F} \approx 99\%$ for many of the problems under investigation.

III. ANGULAR PHASE CONTROL

An attractive feature of nanoscale metadevices is their potential for arbitrary wave-front manipulation under various control variables, including wavelength, polarization, and incident angle. Although spectral and polarization control have been explored in a number of previous works [2,22], to the best of our knowledge, angular control has not been achieved so far. In fact, realizing angular control in traditional single-layer ultrathin metasurfaces might prove fundamentally impossible since the interface is constrained by generalized Snell's laws [1]. On the other hand, MMSs with thicknesses on the order of a wavelength or more (whose internal operation cannot be described via ray optics) can overcome such a limitation; in principle, they can be engineered to exhibit directionality even though conventional approaches which rely on intuitive hand designs might prove unequal to such a task. Here, we leverage our optimization algorithm to develop multifunctional structures where an arbitrary phase response that varies with the angle of incidence can be imprinted on the same device.

The traditional objective in the design of metalenses is the creation of a single hyperbolic phase profile, $\phi(r) = \phi_0 - [(2\pi)/\lambda][\sqrt{f^2 + (r - r_0)^2} - f]$, characterized by the focal length f, in response to a normally incident plane wave [2]. Here, r_0 denotes the center of the lens, whereas ϕ_0 denotes an arbitrary phase reference that can be varied as an additional degree of freedom in the metasurface design [23]. As discussed in Ref. [24], such a design is free of spherical aberrations but still suffers from angular and off-axis aberrations such as coma and field curvature. These errors arise out of an incorrect phase profile that skews the oblique off-axis rays. A corrected phase profile free from aberration is therefore necessarily angle dependent, as given by

$$\phi(r,\theta_{\mathrm{inc}}) = \phi_0(\theta_{\mathrm{inc}}) - \frac{2\pi}{\lambda}\left[\sqrt{f^2 + (r - r_0 - f\tan\theta_{\mathrm{inc}})^2} - f\right].$$

Note that the above expression can be deduced by considering the optical path-length contrast between a generic ray and the orthonormal ray directed towards a focusing spot laterally shifted by $f\tan\theta_{\mathrm{inc}}$ [see Fig. 1(a), blue dashed line]. Here, we leverage our TO algorithm to design a 2D miniature *angle-corrected metalens* that exactly embodies the ideal angle-dependent phase profile given above. Note that, though our miniature design is a proof-of-concept theoretical prototype, it is completely straightforward

(though computationally intensive) to design a full 3D wide-area (centimeter-scale), single-piece, monochromatic, aberration-free lens using our TO technique. We emphasize that such a "next-generation" lens fundamentally differs from the traditional aberration-corrected doublet because the latter exclusively relies on classical ray-tracing techniques, whereas the former intricately exploits nanoscale electromagnetic effects to achieve angular control. On the other hand, it should be noted that, since the performance of our multilayer devices intimately depends on near-field electromagnetic interactions within and between layers, the standard perturbation theory [25] implies that the device will be most sensitive to structural perturbations where the field is strongly concentrated, while, overall, it should be robust roughly up to within a wavelength of misalignment between the layers.

We design a lens with a NA of 0.35 and a focal length of 30λ. The device consists of five layers of topology-optimized aperiodic silicon gratings (invariant along z) against an amorphous alumina background [Fig. 2(a)]. Each silicon layer is 0.2λ thick and is separated by 0.1λ alumina gaps. We specifically choose silicon and alumina with a view to eventual fabrication at mid- or far-IR wavelengths (5–8 μm) by stacking patterned 2D slabs via repeated lithography, material deposition, and planarization processes [26,27]. The entire lens has a thickness of 1.5λ, offering ample space for complex electromagnetic interactions while, at the same time, maintaining orders-of-magnitude-smaller thickness compared to traditional multilens systems. The lens is aberration corrected for four incident angles $\{0°, 7.5°, 15°, 20°\}$, as well as their negative counterparts $\{-7.5°, -15°, -20°\}$ [28]. Note that the largest possible angle for diffraction-limited focusing is approximately 21° and is determined by the numerical aperture. For simplicity, we consider off-axis propagation in the x-y plane with an s-polarized electric field parallel to the direction of the gratings, $\mathbf{E} = E(\mathbf{r})\hat{z}$. A finite-difference time domain (FDTD) analysis of the far field [Fig. 2(b)] reveals focusing action with diffraction-limited intensity profiles [Fig. 2(c)], while the transmission efficiencies

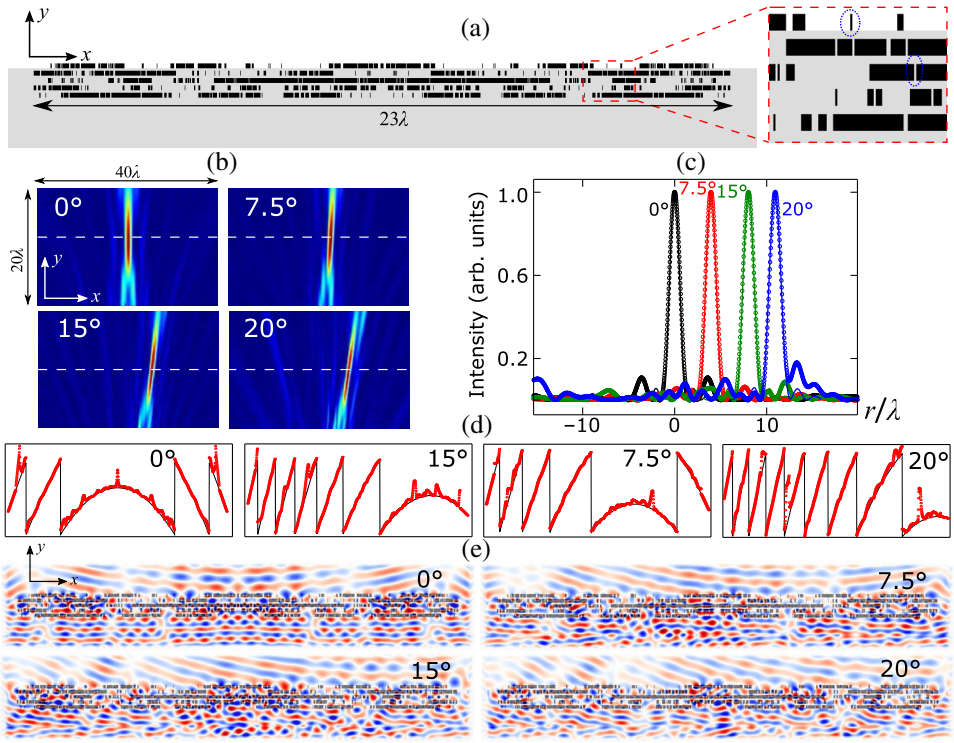

FIG. 2. (a) Multilayered miniature 2D lens (NA = 0.35, $f = 30\lambda$) which is aberration corrected for four incident angles $\{0°, 7.5°, 15°, 20°\}$. Note that, by virtue of symmetry, the lens is automatically corrected for the negative angles as well $\{-7.5°, -15°, -20°\}$. The lens materials consist of five layers of silicon (black) in alumina matrix (gray). (Inset) A portion of the lens is magnified for easy visualization; the smallest features (such as those encircled within the blue dotted oval lines) measure 0.02λ, while the thickness of each layer is 0.2λ. (b) FDTD analysis of the far-field profiles (density plots) reveal focusing action for the four incident angles. Note that the location of the focal plane is denoted by a white dashed line. (c) The field intensities (the circle points) at the focal plane follow the ideal diffraction limit (the solid lines). Note that the intensities are normalized to unity for an easy comparison of the spot sizes. (d) The corresponding phase profile (the red circle data points) for each angle is measured at a distance of 1.5λ from the device, showing good agreement with the ideal profile (the black solid line). (e) Near-field profiles with almost perfect outgoing spherical wave fronts.

average around 25% for the four angles. To evaluate the deviation of our design from the ideal phase profile, we compute the wave aberration function (WAF) for each angle [24], obtaining $\mathrm{WAF}(0°, \pm 7.5°, \pm 15°, \pm 20°) = (0.07, 0.04, 0.06, 0.08)$, which clearly satisfies the Maréchal criterion $\mathrm{WAF} \leq \frac{1}{14}$, except for the 20° incident angle. The errors in the latter case primarily arise from the difficulty over optimizing the extremities of the lens, which can be mitigated by extending the optimized lens area (or, equivalently, designing a larger NA). It is worth noting that the residual phase errors apparent in the optimized design primarily stem from a need to force the optimal design to be binary while being constrained by a limited resolution. In this work, we implement a spatial resolution step size $\Delta r = \lambda/50$ over a 23λ-long simulation domain, while our optimization algorithm handles approximately 5600 degrees of freedom. These parameters are solely dictated by the limited computational resources currently available to us. We find that, without the binary constraint (i.e., when each DOF is allowed to take intermediate values between 0 and 1), the optimal designs easily achieve perfect phase profiles with WAFs smaller than 0.01. We expect that, given better computational facilities, optimization over higher resolution domains will lead to fully binary structures that also preserve vanishing $\mathrm{WAF} \approx 0$.

Next, to demonstrate the versatility of our approach, we design a 2D metalens that focuses light onto the same spot regardless of the angle of incidence [Fig. 1(b)]—a device which we will choose to call *angle-convergent metalens*. Specifically, we impose the phase profile $\phi(r) = \phi_0(\theta_{\mathrm{inc}}) - [(2\pi)/\lambda][\sqrt{f^2 + (r - r_0)^2} - f]$ on the outgoing field under multiple discrete incident angles $\{0°, \pm 3°, \pm 6°, \pm 9°\}$. The lens has a NA of 0.35 and a focal length of 30λ. The lens materials consist of ten layers of 0.05λ-thick silicon in silica separated by 0.05λ gaps [Fig. 3(a)], making the entire device approximately 1λ thick. Such a device can be fabricated using advanced 3D photonic integration techniques [26], including those enabled by CMOS foundries [29]. A far-field analysis [Fig. 3(b)] shows focusing action at the same focal spot for all of the angles. Although the field intensities at the focal spot do not exactly follow the profile of an ideal Airy disk due to residual phase errors, their bandwidth (also known as full width at half maximum) clearly satisfies the diffraction limit [Fig. 3(c)]. The diffraction-limited focusing is also consistent with small WAFs which are found to satisfy the Maréchal criterion:

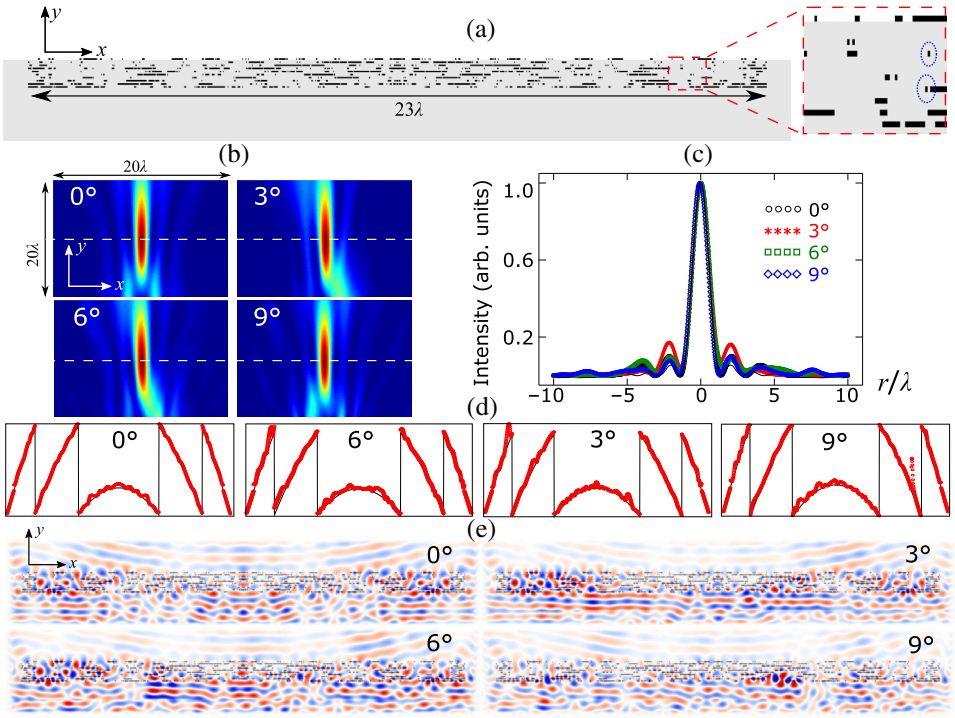

FIG. 3. (a) Multilayered miniature 2D lens (NA = 0.35, $f = 30\lambda$) that exhibits on-axis focusing for the incident angles $\{0°, \pm 3°, \pm 6°, \pm 9°\}$. The lens materials consist of ten layers of silicon (black) in silica matrix (gray). (Inset) A portion of the lens is magnified for easy visualization; the smallest features (such as those encircled within blue dotted oval lines) measure 0.02λ, while the thickness of each layer is 0.05λ. (b) FDTD analysis of the far-field profiles (density plots) reveal the same focal spot for the different incident angles. Note that the location of the focal plane is denoted by a white dashed line. (c) The intensities (symbolic data points) at the focal plane follow the on-axis ideal diffraction limit for all of the incident angles (the solid line). (d) The corresponding phase profile (the red circle data points) for each angle is measured at a distance of 1.5λ from the device, showing good agreement with the ideal profile (the black solid line). (e) Near-field profiles with almost perfect outgoing spherical wave fronts.

$\mathrm{WAF}(0°, \pm 3°, \pm 6°, \pm 9°) = (0.02, 0.04, 0.04, 0.02) < 1/14$. The transmission efficiency of the device averages around 15% over all angles.

IV. CONCLUSION AND OUTLOOK

To summarize, we propose in this paper a general optimization framework for the inverse design of multilayered metaoptics. We leverage our formulation to engineer angular phase control in a multilayered metalens. It is important to note that, in this paper, as we focus on establishing the validity and versatility of our optimization approach via "proof-of-concept" 2D designs, we do not seek to pursue the "best possible practical device" for any particular problem that we choose to investigate. For example, the number, positioning, and thicknesses of layers are arbitrarily chosen in each problem. It is entirely possible that, depending on the desired level of performance, one can achieve viable designs using fewer and/or thicker layers, which could render the entire device even thinner and easier to fabricate. Furthermore, it is conceptually straightforward to design a full 3D device by setting up a collection of parallel disjoint tasks, with each optimizing a sizable fraction of the device that can be managed by an efficient frequency-domain electromagnetic solver [30]. Though by no means infeasible, such an undertaking does require significantly more computational resources than are currently available to us and will be pursued in future works.

While the optimization framework we propose exclusively focuses on phase, work is currently under way to implement additional features such as amplitude uniformity and high-efficiency constraints, which can be straightforwardly added to our formulation. Although the addition of extra conditions would presumably strain the optimization process, we expect that a full 3D multilayered device platform should be able to accommodate any additional demands. In particular, expanding to 3D means another huge leap in the number of degrees of freedom available, which might even make the optimization process easier [31]. With more DOFs, more constraints can be added, such as a constraint requiring that transmission be more than a desired percentage. Furthermore, it is well known that backscattering may be eliminated by specific modal interactions, such as balanced electric and magnetic dipoles [32]. Within the scope of 3D TO, such interactions may be readily inverse designed [19]. Ultimately, we surmise that multilayered volumetric structures (no more than a few wavelengths thick) will help deliver unprecedented wavefront manipulation capabilities at the nanoscale that involve phase, intensity, and polarization control, as well as spectral and angular dispersion engineering *altogether* in a single device. The TO technique is by far the most efficient tool that can handle the enormous design space available to such platforms. Although the fabrication of multilayered nanostructures might prove to be challenging for shorter operational wavelengths, it can be readily implemented in mid- to far-IR regimes through state-of-the-art 3D fabrication technologies [26] such as two-photon lithography [33] and laser writing processes [34], advanced foundry access [29], and ultrahigh-resolution EUV lithography [35].

[1] N. Yu, P. Genevet, M. A. Kats, F. Aieta, J.-P. Tetienne, F. Capasso, and Z. Gaburro, Light propagation with phase discontinuities: Generalized laws of reflection and refraction, Science **334**, 333 (2011).

[2] F. Aieta, M. A. Kats, P. Genevet, and F. Capasso, Multiwavelength achromatic metasurfaces by dispersive phase compensation, Science **347**, 1342 (2015).

[3] A. Arbabi, Y. Horie, M. Bagheri, and A. Faraon, Dielectric metasurfaces for complete control of phase and polarization with subwavelength spatial resolution and high transmission, Nat. Nanotechnol. **10**, 937 (2015).

[4] M. Khorasaninejad, W. T. Chen, R. C. Devlin, J. Oh, A. Y. Zhu, and F. Capasso, Metalenses at visible wavelengths: Diffraction-limited focusing and subwavelength resolution imaging, Science **352**, 1190 (2016).

[5] N. M. Estakhri and A. Alù, Wave-Front Transformation with Gradient Metasurfaces, Phys. Rev. X **6**, 041008 (2016).

[6] A. Arbabi and A. Faraon, Fundamental limits of ultrathin metasurfaces, Sci. Rep. **7**, 43722 (2017).

[7] B. Groever, W. T. Chen, and F. Capasso, Meta-lens doublet in the visible region, Nano Lett. **17**, 4902 (2017).

[8] A. Arbabi, E. Arbabi, S. M. Kamali, Y. Horie, S. Han, and A. Faraon, Miniature optical planar camera based on a wide-angle metasurface doublet corrected for monochromatic aberrations, Nat. Commun. **7**, 13682 (2016).

[9] C. Y. Kao, S. Osher, and E. Yablonovitch, Maximizing band gaps in two-dimensional photonic crystals by using level set methods, Appl. Phys. B **81**, 235 (2005).

[10] J. S. Jensen and O. Sigmund, Topology optimization for nano-photonics, Laser Photonics Rev. **5**, 308 (2011).

[11] K. Svanberg, A class of globally convergent optimization methods based on conservative convex separable approximations, SIAM J. Optim. **12**, 555 (2002).

[12] S. G. Johnson, The NLopt nonlinear-optimization package, http://ab-initio.mit.edu/nlopt (2014).

[13] X. Liang and S. G. Johnson, Formulation for scalable optimization of microcavities via the frequency-averaged local density of states, Opt. Express **21**, 30812 (2013).

[14] J. Lu and J. Vučković, Nanophotonic computational design, Opt. Express **21**, 13351 (2013).

[15] H. Men, K. Y. Lee, R. M. Freund, J. Peraire, and S. G. Johnson, Robust topology optimization of three-dimensional photonic-crystal band-gap structures, Opt. Express **22**, 22632 (2014).

[16] A. Y. Piggott, J. Lu, K. G. Lagoudakis, J. Petykiewicz, T. M. Babinec, and J. Vučković, Inverse design and demonstration of a compact and broadband on-chip wavelength demultiplexer, Nat. Photonics **9**, 374 (2015).

[17] B. Shen, P. Wang, R. Polson, and R. Menon, An integrated-nanophotonics polarization beamsplitter with $2.4 \times 2.4\ \mu\mathrm{m}^2$ footprint, Nat. Photonics **9**, 378 (2015).

[18] Z. Lin, X. Liang, M. Lončar, S. G. Johnson, and A. W. Rodriguez, Cavity-enhanced second-harmonic generation via nonlinear-overlap optimization, Optica **3**, 233 (2016).
[19] Z. Lin, A. Pick, M. Lončar, and A. W. Rodriguez, Enhanced Spontaneous Emission at Third-Order Dirac Exceptional Points in Inverse-Designed Photonic Crystals, Phys. Rev. Lett. **117**, 107402 (2016).
[20] Z. Lin, L. Christakis, Y. Li, E. Mazur, A. W. Rodriguez, and M. Lončar, Topology-optimized dual-polarization Dirac cones, Phys. Rev. B **97**, 081408 (2018).
[21] D. Sell, J. Yang, S. Doshay, R. Yang, and J. A. Fan, Large-angle, multifunctional metagratings based on freeform multimode geometries, Nano Lett. **17**, 3752 (2017).
[22] J. P. B. Mueller, N. A. Rubin, R. C. Devlin, B. Groever, and F. Capasso, Metasurface Polarization Optics: Independent Phase Control of Arbitrary Orthogonal States of Polarization, Phys. Rev. Lett. **118**, 113901 (2017).
[23] M. Khorasaninejad, Z. Shi, A. Y. Zhu, W.-T. Chen, V. Sanjeev, A. Zaidi, and F. Capasso, Achromatic metalens over 60 nm bandwidth in the visible and metalens with reverse chromatic dispersion, Nano Lett. **17**, 1819 (2017).
[24] F. Aieta, P. Genevet, M. Kats, and F. Capasso, Aberrations of flat lenses and aplanatic metasurfaces, Opt. Express **21**, 31530 (2013).
[25] J. D. Joannopoulos, S. G. Johnson, J. N. Winn, and R. D. Meade, *Photonic Crystals: Molding the Flow of Light* (Princeton University Press, Princeton, NJ, 2011).
[26] N. Sherwood-Droz and M. Lipson, Scalable 3D dense integration of photonics on bulk silicon, Opt. Express **19**, 17758 (2011).
[27] M. Qi, E. Lidorikis, P. T. Rakich, S. G. Johnson, J. Joannopoulos, E. P. Ippen, and H. I. Smith, A three-dimensional optical photonic crystal with designed point defects, Nature (London) **429**, 538 (2004).
[28] See Supplemental Material at http://link.aps.org/supplemental/10.1103/PhysRevApplied.9.044030 for further details on the optimized lenses.
[29] M. Hochberg and T. Baehr-Jones, Towards fabless silicon photonics, Nat. Photonics **4**, 492 (2010).
[30] W. Shin, FD3D website, https://github.com/wsshin/fd3d (2015).
[31] N. A. Gershenfeld, *The Nature of Mathematical Modeling* (Cambridge University Press, Cambridge, England, 1999), p. 166.
[32] R. Alaee, R. Filter, D. Lehr, F. Lederer, and C. Rockstuhl, A generalized Kerker condition for highly directive nano-antennas, Opt. Lett. **40**, 2645 (2015).
[33] T. Gissibl, S. Thiele, A. Herkommer, and H. Giessen, Two-photon direct laser writing of ultracompact multi-lens objectives, Nat. Photonics **10**, 554 (2016).
[34] F. Niesler and Y. Tanguy, 3D printers for the fabrication of micro-optical elements, Opt. Photonik **11**, 44 (2016).
[35] C. W. Gwyn, R. Stulen, D. Sweeney, and D. Attwood, Extreme ultraviolet lithography, J. Vac. Sci. Technol. B **16**, 3142 (1998).